Ketogenic diet attenuates Müller cell activation and retinal neuroinflammation in autoimmune glaucoma through acetylation-mediated FOXO signalling

SISI TAN[1*], XIAOCHEN WANG[1*], YUNFAN ZHENG[1], ZHENNI MOU[1], LIHONG ZENG[1,2], JINGCHANG YUAN[1], XIAO FAN[1], MIAO WEI[1], YUJIA HUO[1], RUOTONG OUYANG[1], YANYU PU[1], JUNQIN LEI[1], XI GAO[1], DANGDANG WANG[1], YANG PENG[1] and HONG LI[1]

[1]Department of Ophthalmology, Chongqing Key Laboratory for The Prevention and Treatment of Major Blinding Eye Diseases, The First Affiliated Hospital of Chongqing Medical University, Chongqing 400016, P.R. China; [2]Department of Ophthalmology, Women and Children's Hospital of Chongqing Medical University, Chongqing Health Center for Women and Children, Chongqing 401147, P.R. China

Received April 8, 2026; Accepted August 31, 2026

DOI: 10.3892/ijmm.2026.5992

Abstract. Glaucoma consists of a group of neurodegenerative diseases characterized by retinal ganglion cell degeneration, in which Müller cells are increasingly recognised as drivers of neuroinflammation. A ketogenic diet (KD) elevates circulating β-hydroxybutyrate (BHB) and exhibits benefits in other neurodegenerative disorders; however, its role in glaucoma remains poorly understood. In the present study, an experimental autoimmune glaucoma (EAG) mouse model was established and primary Müller cells were cultured. Using spectrophotometry, optical coherence tomography and immunofluorescence, serum ketone body levels were found to be significantly lower in both patients with primary open-angle glaucoma and EAG mice, independent of intraocular pressure. *In vitro* and *in vivo* experiments showed that KD increased BHB levels and ketone body metabolism, suppressed Müller cell activation and reduced retinal neuroinflammation. In addition, 4D data-independent acquisition proteomic analysis and subsequent validation revealed that FOXO3A acetylation and FOXO3A and metallothionein 2A upregulation were regulated in the retina and Müller cells. These findings suggest that impaired ketone body metabolism occurs in glaucoma and that KD-mediated neuroprotection is associated with altered FOXO3A acetylation. The present study highlighted an association between ketone metabolism and immune regulation in glaucoma, providing evidence for Müller cell phenotypic modulation and supported further investigation of KD as a potential neuroprotective adjunct therapy for glaucoma.

Correspondence to: Professor Hong Li, Department of Ophthalmology, Chongqing Key Laboratory for The Prevention and Treatment of Major Blinding Eye Diseases, The First Affiliated Hospital of Chongqing Medical University, 1 Youyi Road, Yuzhong, Chongqing 400016, P.R. China
E-mail: lihong@hospital.cqmu.edu.cn

*Contributed equally

Abbreviations: RGCs, retinal ganglion cells; BHB, β-hydroxybutyrate; AcAc, acetoacetic acid; PAOG, primary open-angle glaucoma; PACG, primary angle-closure glaucoma; EAG, experimental autoimmune glaucoma; ONA, optic nerve antigen; KD, ketogenic diet; CD, control diet; 4D-DIA, 4D data-independent acquisition; OCT, optical coherence tomography; GS, glutamine synthetase; GCL, ganglion cell layer; MCTs, monocarboxylate transporters; OXCT1, 3-oxoacid CoA-transferase 1; GFAP, glial fibrillary acidic protein; MT2A, metallothionein 2A

Key words: ketogenic diet, neuroinflammation, β-hydroxybutyrate, Müller cell, FOXO3A acetylation, metallothionein 2A, glaucoma

Introduction

Glaucoma, a leading cause of irreversible blindness worldwide, is characterized by progressive apoptosis and degeneration of retinal ganglion cells (RGCs) (1). With a prevalence of 3.54% among the global population aged 40-80 years, the number of affected individuals is projected to reach 111.8 million by 2040 (2). Lowering intraocular pressure (IOP) is a primary therapy for delaying the progression of visual field loss (3). However, progressive visual field deterioration often continues despite therapeutic IOP control, suggesting pressure-independent mechanisms in glaucomatous neurodegeneration (4). Accumulating clinical evidence has indicated that the immune response serves a notable role in the pathogenesis of glaucomatous optic neuropathy (5-7), however, studies in this area remain limited.

Owing to the immune-privileged nature of the retina, retinal glial cells serve as immunocompetent cells within the retina (5). Among these, Müller cells are the predominant subtype, constituting ~90% of the total glial population (8). Under physiological conditions, Müller cells are integral to retinal homeostasis, providing vital structural and metabolic support to neurons (9). During the early stages of glaucoma,

Müller cells are activated by pathological stimulation and exert neuroprotective effects by releasing neurotrophic factors and antioxidants (10). However, sustained Müller cells activation drives the release of pro-inflammatory factors, including TNF-α, ILs and nitric oxide, which in turn initiate excitotoxic insult and ultimately lead to RGC loss (11,12). Existing research has suggested that suppressing Müller cell activation can effectively mitigate neuroinflammation and attenuate RGC loss in glaucoma (13). Despite this, the endogenous regulators capable of modulating Müller cell activation and phenotype switching remain largely unexplored.

Identifying endogenous molecules that can modulate Müller cell activation represents a promising strategy for glaucoma neuroprotection. A ketogenic diet (KD) is a dietary regimen characterised by a minimal carbohydrate, high-fat and moderate protein intake (14). Under this dietary condition, the body uses ketone bodies, including β-hydroxybutyrate (BHB), acetoacetate (AcAc) and acetone, as its primary fuel (15). Among these ketone bodies, BHB is one of the key circulating ketone body metabolites *in vivo* after KD intervention (16,17). Originally a key therapy in epilepsy management, KD has exhibited therapeutic potential in neurodegenerative diseases, including Parkinson's disease and Alzheimer's disease (18). Emerging evidence has indicated that BHB functions as an important signalling molecule and epigenetic modulator, acting as an inhibitor of histone deacetylases to regulate post-translational protein modifications and as a ligand for G protein-coupled receptor 109A to modulate metabolism and inflammatory diseases (19,20). In neurodegenerative diseases, BHB reduces the pathological changes of Alzheimer's disease by inhibiting NLR family pyrin domain containing 3 inflammasome activation (21) and effectively inhibits myelin loss in multiple sclerosis (22). A recent study indicated that BHB mitigates neuroinflammation by reducing microglial activation and pro-inflammatory cytokine (IL-6, IL-1β and TNF-α) levels (23). Despite these promising findings in other neurodegenerative conditions, research regarding BHB in ophthalmology, particularly its effects on Müller cells in glaucoma, remains limited.

The present study aimed to investigate the effects of KD on retinal neuroinflammation and RGC injury in an experimental autoimmune glaucoma (EAG) mice model and identify the underlying molecular mechanisms, with a specific focus on acetylation-mediated FOXO signalling. Through KD intervention in EAG mice, BHB treatment in primary Müller cells and 4D data-independent acquisition (4D-DIA) proteomic analysis, the present study characterized the association between KD/BHB, FOXO3A acetylation and metallothionein 2A (MT2A) upregulation. Furthermore, the potential association between ketone body metabolism and immune regulation in glaucoma was explored, thus providing a theoretical basis for metabolism-based neuroprotective strategies.

Materials and methods

Participants. Guiding principles of the Declaration of Helsinki were strictly followed in all present procedures. All human participants were recruited from the Department of Ophthalmology, The First Affiliated Hospital of Chongqing Medical University (Chongqing, China). Serum samples were collected between March 2024 and October 2025. The entire study protocol was approved by the Ethics Committee of the First Affiliated Hospital of Chongqing Medical University (Chongqing, China; approval no. 2024-087-01). Written informed consent was obtained from all participants involved in the research.

To investigate the differences in ketone body levels between open-angle and angle-closure glaucoma, 15 patients with primary open-angle glaucoma (POAG), 15 patients with primary angle-closure glaucoma (PACG) and 17 age- and sex-matched healthy controls were initially enrolled and analyzed. To further evaluate the effect of IOP on ketone body levels specifically within POAG, an additional 15 POAG patients were enrolled, expanding the total POAG cohort to 30 individuals. These 30 patients were subsequently stratified by baseline IOP into a high-IOP POAG subgroup (POAG-H; IOP >21 mmHg; n=15) and a normal-IOP POAG subgroup (POAG-N; IOP ≤21 mmHg; n=15) (24). For the subgroup comparison, 15 of the 17 original controls were selected through 1:1 matching based on age and sex to serve as the matched reference group. The two unmatched controls were excluded from the subgroup analyses but remained in the initial three-group comparison. Visual field defects were assessed using a Humphrey Field Analyzer (Carl Zeiss AG) with the 24-2 Swedish Interactive Thresholding Algorithm standard strategy (25). Peripheral blood samples were collected from each participant and processed to isolate serum, which was stored at -80˚C. Patients with a clinical diagnosis of glaucoma (including both POAG and PACG), confirmed by at least two experienced ophthalmologists, aged ≥18 years and capable of providing written informed consent, were enrolled in this study. Patients with glaucoma of any disease duration, regardless of prior treatment status, were included. Individuals with other ocular diseases (such as diabetic retinopathy and age-related macular degeneration), hypertension, diabetes mellitus, systemic infections or any condition that could affect systemic metabolism were excluded. The present study enrolled 62 participants (32 men and 30 women), with a median age of 65 (range: 50-81 years). The details for each group, including the numbers sex distribution, median age and age range, are summarized in Table SI. Detailed clinical characteristics and visual field parameters for the POAG-H and POAG-N subgroups are presented in Table SII.

Mice and immunization. All animal procedures were approved by the Institutional Animal Care and Use Committee of Chongqing Medical University (Chongqing, China; approval no. IACUC-CQMU-2025-0349) and performed in compliance with the Association for Research in Vision and Ophthalmology guidelines (26). A total of 72 adult male C57BL/6J mice (6-8 weeks old) were used in the present study, with 15 being used for the pre-experiment. Mice were divided into a control group (CON; n=3) and an EAG group (12 mice, subdivided into four time points at weeks 2, 4, 6 and 8; n=3 each). Due to the limited amount of retinal tissue obtained from each mouse, to ensure a sufficient sample size for multiple assays (n=3-6 per group), 57 mice were used for the formal experiments, including the CON group (6 mice), the EAG group (6 mice), the CON + control diet group (15 mice),

the EAG + control diet group (15 mice) and the EAG + KD group (15 mice). The exact n values for each specific assay are indicated in the corresponding figure legends.

Mice were obtained from the Experimental Animal Center of Chongqing Medical University (Chongqing, China) and housed in a pathogen-free environment. EAG was induced as previously described (27,28). Briefly, fresh bovine eyes were obtained from a local slaughterhouse (Chongqing, China) for optic nerve antigen (ONA) extraction, ground at -30˚C and then suspended in PBS (cat. no. BL601A; Biosharp Life Sciences) to obtain a suspension with a concentration of 1 mg/ml. For immunization, the mice received an intraperitoneal injection of 50 μl ONA emulsified with the same volume of incomplete Freund's adjuvant (FA) (cat. no. P2031; Beyotime Biotechnology), supplemented with 1 μg pertussis toxin (PTX; cat. no. P7208; Sigma-Aldrich; Merck KGaA). A total of 2 days later, these mice received another injection of PTX (1 μg) through the same route. PTX was administered to ensure the permeability of the blood-retinal barrier as previously described (27). The control mice received intraperitoneal injection of 100 μl PBS, FA and PTX.

For the pre-experiment, mice were euthanized at weeks 2, 4, 6 and 8 post-immunization to monitor disease progression and determine the optimal endpoint for therapeutic evaluation. For formal experiments, all mice were euthanized at week 4 post-immunization. At each designated time point, serum samples (~100 μl) and retinal tissues were harvested for subsequent analysis. For blood collection, mice were deeply anesthetized with tribromoethanol (250 mg/kg; cat. no. 2092A; Nanjing Aibei Biological Technology Co., Ltd.) administered through intraperitoneal injection. Following the induction of deep anesthesia (determined by the loss of pedal withdrawal reflex), blood was collected by enucleation of the eyeball. Immediately following blood collection, mice were subsequently euthanized through cervical dislocation. Mortality was determined by the complete cessation of heartbeat and respiration, as well as the absence of all reflexes. Retinal tissues were then harvested immediately after euthanasia. Serum was separated from whole blood samples by centrifugation (100 x g for 20 min at room temperature) and stored at -80˚C until further analysis. Blood samples and retinal tissues were collected from separate cohorts of mice at each time point and all mice were euthanized immediately after each sample collection.

Mice diets. Semi-purified diets, including a KD (cat. no. D10070801) and a control diet (CD; cat. no. D10070802), were purchased from Ready Dietech (Shenzhen) Co., Ltd. Their detailed compositions are provided in Table SIII. Immunized mice were randomly assigned to two groups and fed *ad libitum* for 4 weeks with either an irradiated KD (EAG-KD) or an irradiated CD (EAG-CD). A separate cohort of non-immunized mice was fed the CD (CON-CD) to serve as a negative control. Upon termination of the present study, retinal tissues and serum samples were collected from all mice for further experimental procedures.

Cell culture and cell treatments. All procedures were supported by the Institutional Animal Care and Use of Chongqing Medical University (Chongqing, China; approval no. IACUC-CQMU-2025-0349) and in compliance with Association for Research in Vision and Ophthalmology guidelines. The culture procedures for primary Müller cells followed a previously published report with minor modifications (29). Briefly, Müller cells were isolated from retinas of 5-day-old C57BL/6J mice (mixed-sex neonatal mice). Based on the present preliminary optimization experiments, retinas from 8 neonatal mice were pooled and seeded into a single T75 culture flask, which consistently yielded sufficient cell numbers with high purity after passaging. To ensure experimental reproducibility, four independent isolations were performed for the present study, using a total of 32 neonatal mice.

Neonatal mice were euthanized by cervical dislocation before tissue collection. Mortality was determined by complete cessation of heartbeat and respiration, as well as absence of reflexes. Following dissection, retinal pieces were digested in 0.25% trypsin (cat. no. 25200072; Gibco; Thermo Fisher Scientific, Inc.) for 3-5 min at 37˚C to obtain separate cells. Dissociated cells were seeded into poly-d-lysine (cat. no. P2100; Beijing Solarbio Science & Technology Co., Ltd.) pre-coated 75 cm^2 flasks, and then maintained in DMEM (cat. no. 11965092; Gibco; Thermo Fisher Scientific, Inc.) containing 20% FBS (cat. no. NEW500; Serana Biologicals) and 1% penicillin-streptomycin (cat. no. C0222; Beyotime Biotechnology) under standard conditions (37˚C and 5% CO_2). Medium changes were performed at intervals of 3-4 days. The culture medium was replaced twice a week. Subsequently, ~10 days later, the cells were passaged at a 1:1 ratio. After 2-3 passages at the same split ratio (1:1), the Müller cells became relatively pure and were identified by cell morphology and immunofluorescence with glutamine synthetase (GS). Müller cells in passages 3-5 were used for the present experiments.

For lipopolysaccharide (LPS; cat. no. L2880; Sigma-Aldrich; Merck KGaA) treatment, Müller cells, seeded in DMEM with 5% FBS, were then subjected to LPS (0, 0.1, 0.5, 1, 2, 5 or 10 μg/ml) for 72 h at 37˚C. For BHB (MedChemExpress; cat. no. HY-113378) treatment, Müller cells maintained in DMEM with 5% FBS were exposed to a range of BHB concentrations (0, 0.5, 1, 2, 5, 10, 20 or 50 mM) for 72 h at 37˚C, with or without co-treatment of 1 μg/ml LPS.

Measurement of ketone bodies. Serum was separated from the peripheral blood of human participants and mice, followed by the measurement of serum concentrations of BHB and acetoacetic acid using a microplate assay kit (cat. no. BC5065; Beijing Solarbio Science & Technology Co., Ltd.) according to the manufacturer's instructions. Briefly, the working solutions of BHB and AcAc were separately mixed with the serum and placed in a 96-well microplate for reaction. The optical density (OD) at 340 nm was measured using a Thermo Scientific Varioskan™ LUX microplate reader (Thermo Fisher Scientific, Inc.) at 37˚C and then statistical calculations were conducted.

Measurement of glucose. Serum was separated from mouse peripheral blood, followed by the measurement of serum glucose concentrations using a colorimetric assay kit (cat. no. G1212W; Suzhou Grace Biotechnology Co., Ltd.) according to the manufacturer's instructions. Briefly, the working solution was mixed with the serum and placed in a 96-well plate at 37˚C in the dark for 30 min. The OD at 510 nm was measured

at 37˚C using a Thermo Scientific Varioskan LUX microplate reader (Thermo Fisher Scientific, Inc.) and then statistical calculations were conducted.

IOP measurements. IOP was measured weekly from 9:00-11:00 AM using a TonoLab rebound tonometer (iCare Finland Oy) until the experimental endpoint. Each recorded value constitutes the mean of six independent IOP measurements, as described in a previous study by the present authors (30).

Optical coherence tomography (OCT). For OCT imaging, general anaesthesia was induced to mice through intraperitoneal injection of tribromoethanol (250 mg/kg). Following anaesthesia, pupils were dilated using compound tropicamide eye drops to enable clear fundus visualization. Mice were subjected to OCT using an Ultramicro Ophthalmol Imaging System (ISOCT; Optoprobe Science Ltd.) for assessment of the ganglion cell layer (GCL) thickness. All OCT scans, performed using the Optoprobe-OCT system, were centred on the posterior pole of the retina. To ensure comparability, scans were consistently acquired from the same retinal location. The system simultaneously captured fundus images during scanning and generated detailed fundus maps. Subsequently, the acquired OCT images were analyzed using the OCT Image Analysis Software (version 2.0; Optoprobe Science Ltd.) to obtain the average GCL thickness. After OCT acquisition, mice were allowed to recover from anaesthesia.

H&E staining. Mouse eyeballs were harvested and immersion-fixed in undiluted FAS Eyeball Fixative Solution (cat. no. G1109; Wuhan Servicebio Technology Co., Ltd.) at room temperature for at least 24 h before paraffin embedding. Consecutive 4-μm sections along the corneal-optic nerve axis were generated. H&E staining was performed at room temperature using the H&E Staining Kit (cat. no. G1076; Wuhan Servicebio Technology Co., Ltd.) according to the manufacturer's standard operating procedures. Briefly, sections were dewaxed in dewaxing solution (cat. no. G1128; Wuhan Servicebio Technology Co., Ltd.) for 15 min twice, rehydrated in graded ethanol (100% ethanol twice, 75% ethanol once, 5 min each; cat. no. 100092683; Sinopharm Chemical Reagent Co., Ltd.), and washed with tap water. Sections were then pretreated with High-Definition Constant Temperature Pretreatment Solution (Servicebio) for 1 min, followed by staining with hematoxylin for 3 min. After washing, sections were differentiated in differentiation solution (Wuhan Servicebio Technology Co., Ltd.) for 5 sec, blued in bluing solution (Wuhan Servicebio Technology Co., Ltd.) for 5 sec and rinsed with tap water. Subsequently, sections were dehydrated in 95% ethanol for 1 min and stained with eosin for 15 sec. Finally, sections were dehydrated through graded ethanol (100% ethanol three times, 1 min each) and n-butanol (cat. no. 100052190; Sinopharm Chemical Reagent Co., Ltd.) twice for 1 min each, cleared in xylene (cat. no. X100301-S5L; Shanghai Lingfeng Chemical Reagent Co., Ltd.) twice for 1 min each, and mounted with neutral balsam (cat. no. 10004160; Sinopharm Chemical Reagent Co., Ltd.) Stained sections were imaged using a conventional light microscope (Leica Microsystems GmbH).

Quantification of RGCs in retinal flat-mounts. Following enucleation, eyeballs were fixed by immersion in FAS Eyeball Fixative Solution for 2 h at room temperature. The retinas were dissected and flat-mounted and then permeabilized with 0.5% Triton X-100 (cat. no. P0096; Beyotime Biotechnology) for 30 min and blocked in a solution containing 5% normal goat serum (cat. no. AR0009; Boster Biological Technology, Co., Ltd.) at room temperature for 1 h. Subsequently, retinas were incubated overnight at 4˚C with the RGC specific marker brain-specific homeobox/POU domain protein 3A (Brn3a; 1:100; cat. no. ab81213; Abcam) and then incubated with a 594-conjugated goat anti-rabbit IgG (H+L) secondary antibody (1:200; cat. no. AS039; ABclonal Biotech Co., Ltd.) at room temperature for 1 h and counterstained with DAPI at room temperature for 5 min (cat. no. P0131; Beyotime Biotechnology) to visualize nuclei. Images were captured on an immunofluorescence microscope (Leica Microsystems, Inc.).

Immunofluorescence staining. Deparaffinized sections (cat. no. G1128; Servicebio) underwent heat-induced epitope retrieval in Tris-EDTA buffer (pH 9.0; 95˚C; 30 min). After blocking with 5% normal goat serum at room temperature for 1 h, sections were probed with primary antibodies against glial fibrillary acidic protein (GFAP; 1:300; cat. no. 60190-1-Ig), monocarboxylate transporter (MCT)-1 (1:200; cat. no. 20139-1-AP), MCT2 (1:300; cat. no. 20355-1-AP) and 3-oxoacid CoA-transferase 1 (OXCT1; 1:200; cat. no. 12175-1-AP; all, Proteintech Group, Inc.) overnight at 4˚C. Detection was achieved using Alexa Fluor 488-goat anti-rabbit (cat. no. A0423) and Alexa Fluor 555-donkey anti-mouse (cat. no. A0460) secondary antibodies (all, 1:500; all, Beyotime Biotechnology) for 1 h at room temperature, followed by DAPI counterstaining at room temperature for 5 min. Images were captured on an immunofluorescence microscope (Leica Microsystems, Inc.).

For the immunofluorescence staining of Müller cells, briefly, cells from passages 2-3 were seeded on glass slides in a 24-well plate for 24 h. After fixation with 4% paraformaldehyde (cat. no. P0099; Beyotime Biotechnology) at 37˚C for 10 min and permeabilization with 0.5% Triton X-100 (cat. no. P0096; Beyotime Biotechnology) at 37˚C for 30 min, samples were blocked with 5% BSA (cat. no. FA016; Genview) at 37˚C for 30 min and incubated overnight at 4˚C with primary antibody against GS (1:200; cat. no. GTX109121; GeneTex, Inc.). Subsequently, cells were incubated with Alexa Fluor 488-conjugated goat anti-rabbit IgG (H+L) (as aforementioned) for 1 h at room temperature. Slides were mounted in anti-fade medium containing DAPI and visualized using an immunofluorescence microscope (Leica Microsystems, Inc.).

Cell viability assay. A Cell Counting Kit-8 (CCK-8; cat. no. HY-K0301; MedChemExpress) was employed to determine cell viability. Following the manufacturer's instructions, 100 μl cells ($1x10^6$ cells/ml) were inoculated into a 96-well plate. The next day, cells were cultured with numerous concentrations (0.1, 0.5, 1, 2, 5 or 10 μg/ml) of LPS at 37˚C for 72 h or treated with various concentrations (0, 0.5, 1, 2, 5, 10, 20 or 50 mM) of BHB with or without 1 μg/ml LPS at 37˚C for 72 h. Following a 2-h incubation with 10 μl CCK-8 solution at 37˚C in the dark,

the OD at 450 nm of Müller cell cultures was quantified using a Varioskan LUX microplate reader (Thermo Fisher Scientific, Inc.). All assays were performed at least three times.

4D-DIA proteomics analysis. Proteomics analysis was performed by Shanghai Applied Protein Technology Co., Ltd. A total of three independent cultures of Müller cells ($2x10^6$ cells per 10 cm dish) were prepared for each group (Control, LPS and LPS + BHB). After 72 h of treatment at 37˚C, the culture medium was removed and cells were washed, scraped and collected into 1.5 ml tubes. After sample collection, samples were lysed in SDC buffer (5% sodium deoxycholate; 100 mM Tris-HCl; pH 8.5), followed by protein reduction and alkylation using 1 mM Tris (2-carboxyethyl) phosphine and 1 mM chloroacetamide, respectively. After spiking with indexed retention time peptides, the samples were analysed using an Evosep One-coupled timsTOF Pro2 mass spectrometer (Bruker Daltonics; Bruker Corporation) in DIA mode. The resulting 4D-DIA data were processed using Spectronaut™ (version 19.7) software (31,32). Proteins exhibiting decreased expression in the LPS group relative to control and increased expression in the LPS + BHB group relative to LPS were first identified. From these, proteins meeting the criteria of fold change >1.2 and P<0.05 in pairwise comparisons were selected for further analysis. The present mass spectrometry proteomics data were deposited in the iProX database (https://www.iprox.cn) under accession no. IPX0018867000.

Reverse transcription quantitative PCR (RT-qPCR). Total RNA was extracted from mouse retinal tissues and cultured Müller cells using Total RNA Isolation Reagent (cat. no. AG21017; Accurate Biotechnology (Hunan) Co., Ltd.). For cDNA synthesis, 500 ng of RNA was first treated with 5X gDNA digester Mix (cat. no. HY-K0511A; MedChemExpress) at 42˚C for 2 min in a 15-μl reaction to remove genomic DNA. Subsequently, 4X Super RT Mix (from the same kit) was added to a final volume of 20 μl, and reverse transcription was performed at 25˚C for 5 min, 55˚C for 15 min and 85˚C for 2 min. The resulting cDNA was stored at 4˚C until use for qPCR. Gene expression was quantified by qPCR on an Applied Biosystems 7500 system using SYBR Green qPCR Master Mix (cat. no. HY-K0522; MedChemExpress). The qPCR cycling conditions were as follows: Initial denaturation at 94˚C for 10 sec; 4 cycles of 50˚C for 30 sec and 72˚C for 1 min; followed by 95˚C for 30 sec; and 42 cycles of 95˚C for 5 sec, 60˚C for 30 sec and 72˚C for 30 sec. Transcript levels for GFAP, IL-1β, IL-6, TNF-α, MCT1, MCT2 and OXCT1 were calculated using the $2^{-\Delta\Delta Cq}$ method relative to β-actin (33). Primer sequences are listed in Table SIV.

Western blotting. Retina and Müller cell proteins were extracted using a lysis buffer composed of RIPA Lysis Buffer (cat. no. P0013B; Beyotime Biotechnology) and PMSF solution (cat. no. ST506; Beyotime Biotechnology) at a ratio of 99:1. Protein concentrations were quantified using a BCA method (cat. no. P0009; Beyotime Biotechnology). Equal amounts of protein (20 μg per lane) were resolved on 4-20% gels using SDS-PAGE (cat. no. F15412MGel; ACE Biotechnology) and transferred to PVDF membranes (cat. no. IPVH00010; MilliporeSigma; Merck KGaA). Blocking was performed using QuickBlock™ Buffer (cat. no. P30500; NCM Biotech) for 20 min at room temperature. Membranes were probed overnight at 4˚C with specific primary antibodies, followed by incubation with secondary antibodies HRP-conjugated Goat Anti-Rabbit IgG(H+L) (1:10,000; cat. no. SA00001-2; Proteintech Group, Inc.) and Dylight 800 Goat Anti-Mouse IgG (1:20,000; cat. no. RS23910; ImmunoWay Biotechnology Company) for 1 h at room temperature. Protein bands were visualized using a Western Bright™ ECL kit (cat. no. HY-K2005; MedChemExpress). The relative protein expression levels were quantified by grayscale analysis using the ImageJ software (version 1.54p; National Institutes of Health). Specifically, the intensity of the acetylated FOXO3A band was normalized to the intensity of the corresponding total FOXO3A band and then further normalized with β-tubulin as the loading control. All steps were performed according to the manufacturers' protocols.

Primary antibodies used included: GFAP (1:3,000; cat. no. 60190-1-Ig; Proteintech Group, Inc.), MCT1 (1:1,000; cat. no. 20139-1-AP; Proteintech Group, Inc.), MCT2 (1:1,000; cat. no. 20355-1-AP; Proteintech Group, Inc.), OXCT1 (1:1,000; cat. no. 12175-1-AP; Proteintech Group, Inc.), IL-1β (1:1,000; cat. no. WL02257; Wanleibio Co., Ltd.), IL-6 (1:1,000; cat. no. WL02841; Wanleibio Co., Ltd.), TNF-α (1:1,000; cat. no. WL01581; Wanleibio Co., Ltd.), acetylated-lysine (1:2,000; cat. no. HA723073; HUABIO), FOXO3A (1:2,000; cat. no. ET1604-11; HUABIO), acetyl-FOXO3A (Lys271; 1:2,000; cat. no. AF3771; Affinity Biosciences), acetyl-FOXO3A (Lys290; 1:1,000; cat. no. AF3770; Affinity Biosciences), MT2A (1:2,000; cat. no. DF6755; Affinity Biosciences), β-actin (1:20,000; cat. no. HA722023; HUABIO) and β-tubulin (1:20,000; cat. no. ET1602-4; HUABIO).

Statistical analysis. All data are presented as the mean ± SD. Statistical analyses were performed using SPSS (version 26.0; IBM, Corp.). GraphPad (version 10.0; Dotmatics) was used to visualize all experimental data. Normality was assessed using the Shapiro-Wilk test. Depending on normality, two-group comparisons were made using unpaired t-tests or Mann-Whitney U tests and multi-group comparisons used one-way ANOVA with Tukey's multiple comparisons test or the Kruskal-Wallis tests with Dunn's post-hoc test. The n values represent the number of samples. A minimum of three independent replicates were included for all experiments. Statistical significance is denoted as follows: *P<0.05, **P<0.01, ***P<0.001 and ****P<0.0001.

Results

Serum ketone body levels decrease in patients with POAG. Serum levels of BHB and AcAc were first measured in patients with POAG, patients with PACG and healthy controls to identify differences among the three groups (Fig. 1A). The POAG group exhibited significantly lower serum ketone body levels compared with the PACG and healthy control groups (Fig. 1B and C). To determine whether decreased serum ketone body levels were associated with IOP in patients with POAG, patients were divided into a POAG-H group (30.87±9.70 mmHg) and a POAG-N group (17.67±1.95 mmHg), based on whether their first IOP measurement on admission was >21 mmHg (Fig. 1D). Levels of BHB and AcAc were significantly reduced

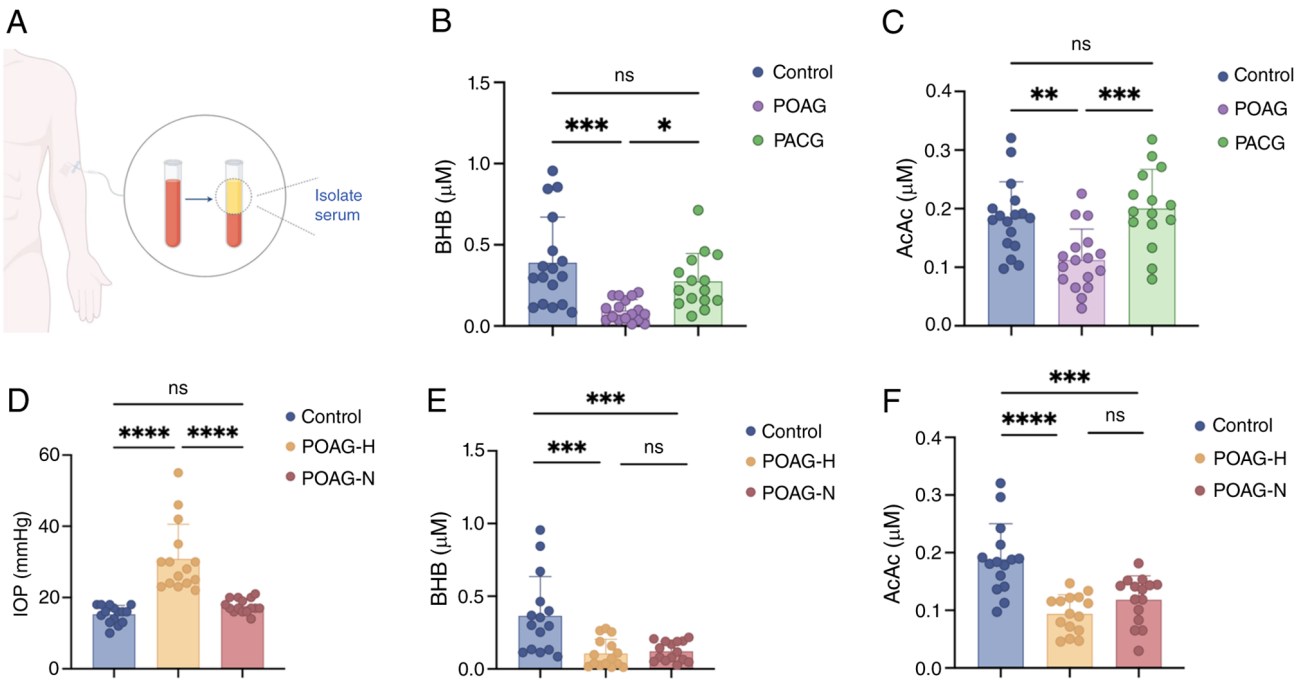

Figure 1. Serum ketone body (BHB and AcAc) levels were reduced in patients with POAG. (A) Schematic diagram of serum sample collection. (B) Serum BHB levels in healthy controls (n=17), POAG patients (n=15) and PACG patients (n=15). (C) Serum AcAc levels in healthy controls (n=17), POAG patients (n=15) and PACG patients (n=15). (D) Comparisons of IOP in healthy controls, POAG-H patients and POAG-N patients (n=15 for three groups). (E) Serum BHB levels in POAG-H patients, POAG-N patients and healthy controls (n=15 for three groups). (F) Serum AcAc levels in POAG-H patients, POAG-N patients and healthy controls (n=15 for three groups). 'n' represents the number of samples. Data are presented as the mean ± SD. One-way ANOVA was used for B-F. *P<0.05, **P<0.01, ***P<0.001 and ****P<0.0001. ns, not significant; BHB, β-hydroxybutyrate; AcAc, acetoacetic acid; POAG, primary open-angle glaucoma; PACG, primary angle-closure glaucoma; IOP, intraocular pressure; POAG-H, high-IOP group; POAG-N, normal-IOP group.

in both the POAG-H and POAG-N groups relative to controls (Fig. 1E and F). Baseline characteristics of the POAG-H and POAG-N groups, including disease duration, medication use and visual field defects, are summarised in Table SII. No significant differences in these parameters were observed between the two subgroups, suggesting that the reduction in ketone body levels was independent of IOP and other clinical confounders.

EAG mice exhibit glaucomatous injury accompanied by decreased serum ketone bodies. Subsequently, an ONA-induced EAG model was employed (Fig. 2A). Quantification of RGCs by immunofluorescence at 2, 4, 6 and 8 weeks after immunization revealed statistically significant RGC loss beginning at week 4 (Fig. S1A). RT-qPCR analysis of IL-1β, IL-6, TNF-α and GFAP at 0, 2 and 4 weeks exhibited progressive upregulation of these markers, with a significant increase at week 4 (Fig. S1B). Collectively, these results demonstrated successful establishment of the EAG model by week 4 and supported its use in subsequent experiments. During the first 4 weeks after immunization, the IOP remained normal in the EAG and the control groups, with no significant differences observed (Fig. 2B). H&E staining and OCT images exhibited significant thinning of the GCL and loss of RGCs in the EAG group compared with controls (Fig. 2C and D). RGC loss was further determined by Brn3a immunostaining, which showed a significant reduction in RGC numbers in the EAG group compared with the control group (Fig. 2E and F). The association between ketone body levels and glaucomatous damage was then examined, revealing significantly lower serum ketone body levels in the EAG group compared with the control group, consistent with observations in POAG (Fig. 2G). These results suggest a possible association between optic nerve injury and reduced serum ketone body levels in EAG mice.

KD enhances the transport and utilization of ketone bodies in the retina of EAG mice. KD feeding was used to increase ketone body levels *in vivo*. EAG mice were fed a CD (80% CHO, 10% protein and 10% fat) or a KD (0% CHO, 10% protein and 90% fat) for 4 weeks (Fig. 3A). Serum ketone body levels were found to be significantly elevated in KD-fed EAG mice compared with those in the CD-fed group (Fig. 3B). ONA immunization did not affect blood glucose levels but resulted in body weight loss in mice. By contrast, KD had no significant effect on either blood glucose levels or body weight in EAG mice (Fig. 3C and D).

To evaluate changes in ketone body transport and utilization in the retina, key enzymes and molecules involved in these processes were examined. The expression of monocarboxylate transporters (MCT1 and MCT2) and OXCT1 was found to be significantly decreased in the retinas of EAG mice compared with healthy controls at both the protein and RNA levels. Following KD intervention, MCT1 and OXCT1 expression increased, whereas MCT2 expression exhibited no significant change (Fig. 3E-I). These results demonstrated that KD increased serum ketone body levels and concurrently upregulated retinal MCT1 and OXCT1 expression in EAG mice.

KD suppresses Müller cell activation and inflammatory factors release and promotes RGC survival. To evaluate the effects of elevated serum ketone bodies on EAG mice, retinal

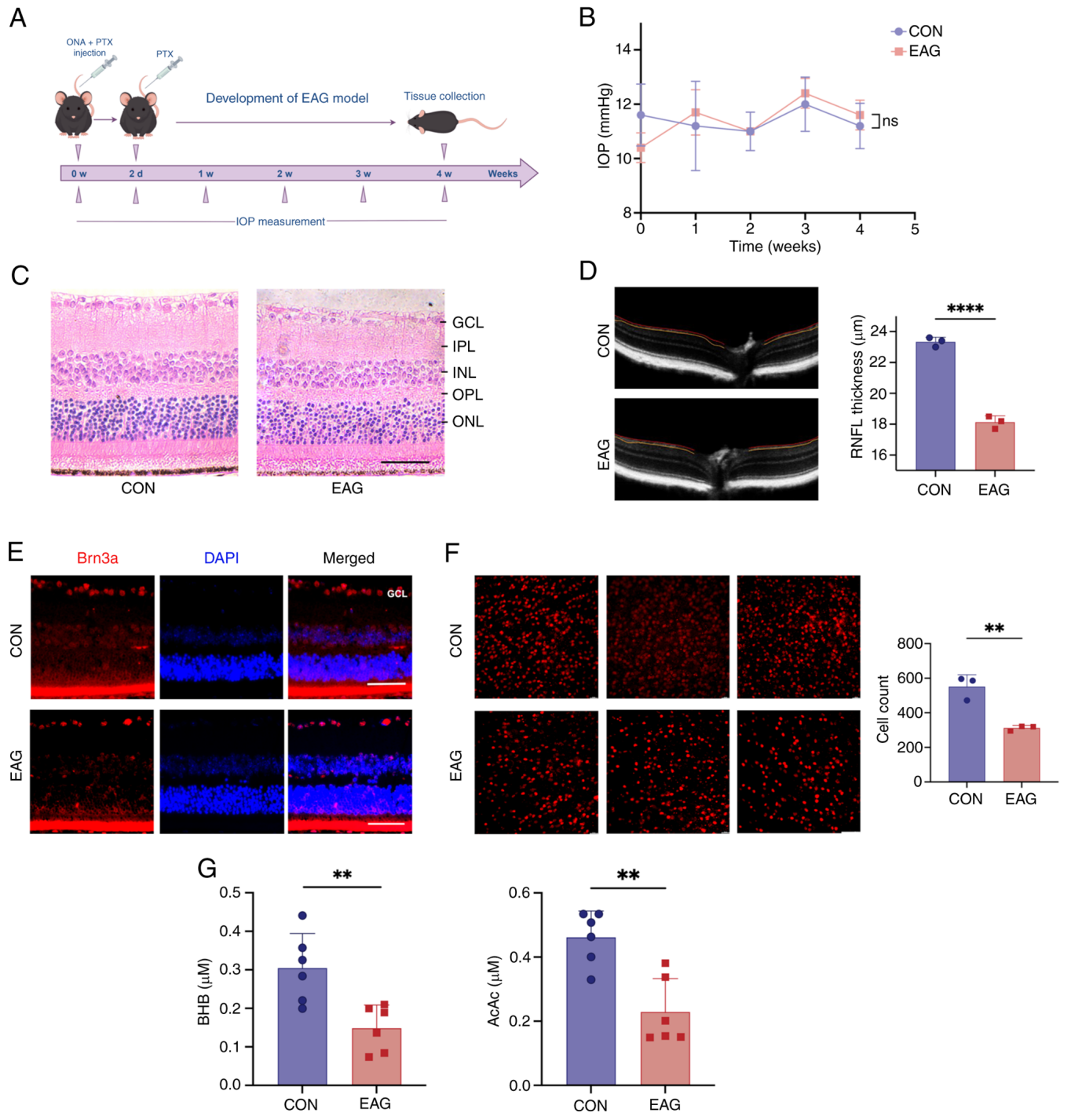

Figure 2. EAG mice exhibit glaucomatous neurodegeneration and decreased serum ketone bodies. (A) Schematic of the EAG mouse model. (B) IOP measurements in CON and EAG groups (n=6 mice for each group). (C) H&E staining of retinal sections in CON and EAG groups. (n=3 mice for each group). (D) Optical coherence tomography analysis and quantification data of RNFL thickness in CON and EAG groups (n=3 mice for each group). (E) Immunofluorescent staining of Brn3a$^+$ cells in the retinal sections of CON and EAG groups. (F) Immunofluorescent staining and quantification data of Brn3a$^+$ cells in the retinal flat mounts of CON and EAG groups (n=3 mice for each group). (G) Serum BHB and AcAc levels in CON and EAG groups (n=6 mice for each group; scale bar, 50 μm). Data are presented as the mean ± SD. Unpaired t-tests were used for (D-G). **P<0.01 and ****P<0.0001. ns, not significant; BHB, β-hydroxybutyrate; AcAc, acetoacetic acid; IOP, intraocular pressure; GCL, ganglion cell layer; IPL, inner plexiform layer; INL, inner nuclear layer; OPL, outer plexiform layer; ONL, outer nuclear layer; RNFL, retinal nerve fibre layer; CON, control; PTX, pertussis toxin; Brn3a, brain-specific homeobox/POU domain protein 3A; EAG, experimental autoimmune glaucoma; ONA, optic nerve antigen.

layer thickness was assessed by H&E staining, with OCT and RGCs being quantified by immunofluorescence. KD-fed EAG mice exhibited increased GCL thickness and significantly elevated RGC numbers compared with the CD-fed EAG group (Fig. 4A-D). A hallmark of Müller cell activation is the upregulation of GFAP (10). Immunofluorescence, western blotting and RT-qPCR analyses revealed significantly increased GFAP expression in the retina of EAG mice compared with the control, which was further significantly reversed by KD feeding (Fig. 4E-H). Similarly, western blotting and RT-qPCR

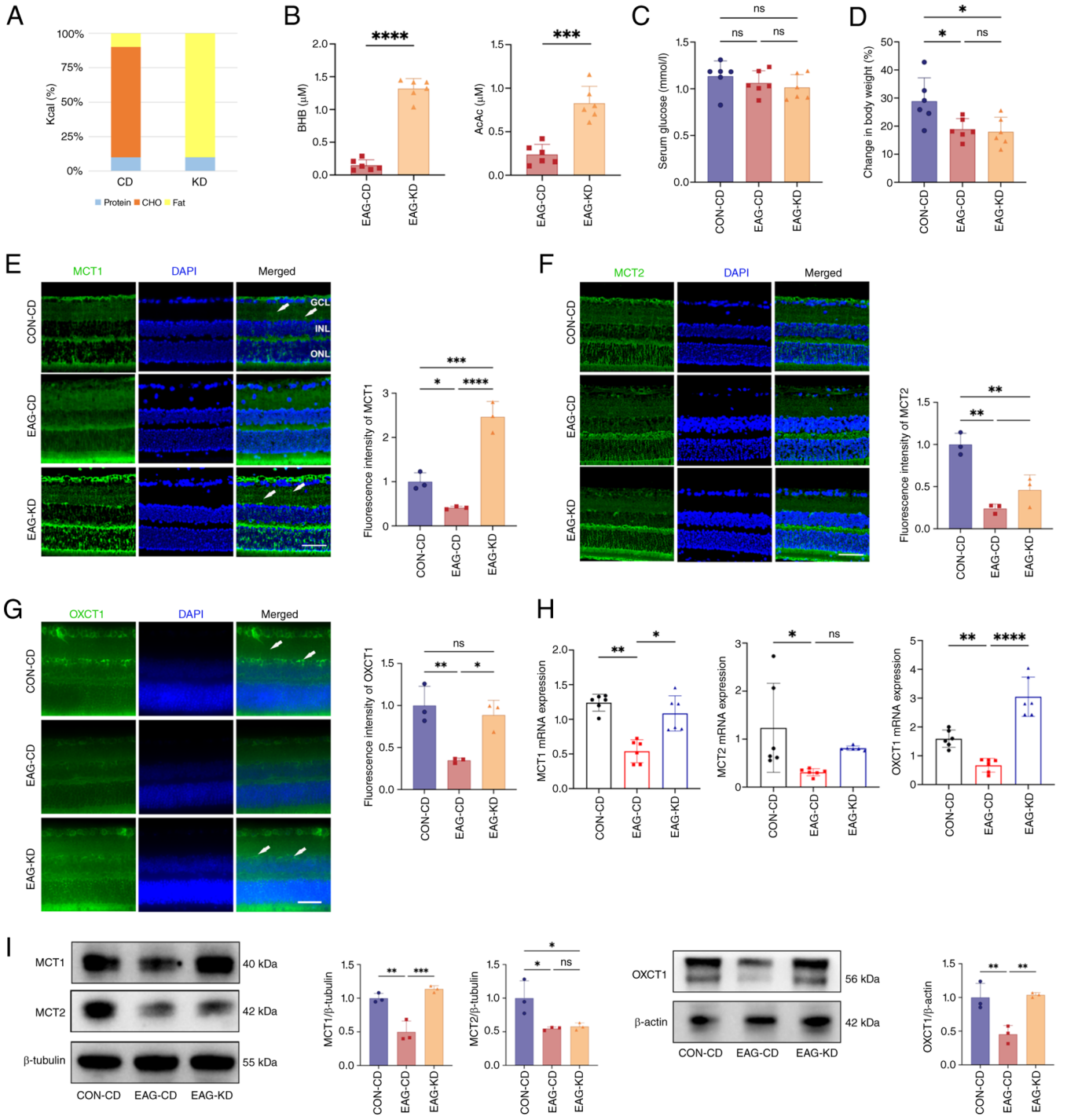

Figure 3. KD feeding enhances ketone body transportation and utilization in the retina of EAG mice. (A) Composition formulation of the CD and KD. (B) Serum BHB and AcAc levels in EAG-CD and EAG-KD groups (n=6 mice for each group). (C) Serum glucose levels in EAG-CD and EAG-KD groups (n=6 mice for each group). (D) Body weight changes during the experimental period in CON-CD, EAG-CD and EAG-KD groups (n=6 mice for each group). (E) Immunofluorescent staining and quantification data of MCT1 in retinal sections of CON-CD, EAG-CD and EAG-KD groups (n=3 mice for each group; white arrows indicate MCT1$^+$ staining). (F) Immunofluorescent staining and quantification data of MCT2 in retinal sections of CON-CD, EAG-CD and EAG-KD groups (n=3 mice for each group). (G) Immunofluorescent staining and quantification of OXCT1 in retinal sections of CON-CD, EAG-CD and EAG-KD groups (n=3 mice for each group; white arrows indicate OXCT1$^+$ staining). (H) Relative mRNA expression of MCT1, MCT2 and OXCT1 in the retinas of CON-CD, EAG-CD and EAG-KD groups (n=6 mice for each group). (I) Western blotting analysis and quantification of MCT1, MCT2 and OXCT1 protein expressions in the retinas of CON-CD, EAG-CD and EAG-KD groups (n=3 mice for each group; scale bar, 50 μm). Data are presented as the mean ± SD. Unpaired t-tests were used for (B). One-way ANOVA and Kruskal-Wallis were used for (C-I). *P<0.05, **P<0.01, ***P<0.001 and ****P<0.0001. ns, not significant; KD, ketogenic diet; EAG, experimental autoimmune glaucoma; CD, control diet; BHB, β-hydroxybutyrate; EAG-KD, irradiated KD; EAG-CD, irradiated CD; MCT, monocarboxylate transporter; OXCT1, 3-oxoacid CoA-transferase 1; CHO, carbohydrate.

analyses showed significantly elevated expression of IL-1β, IL-6 and TNF-α in the retina of EAG mice, with KD feeding further significantly reducing their levels (Fig. 4I and J). These findings indicate that KD was associated with suppressed Müller cell activation, reduced inflammatory factor expression and improved RGC survival in the EAG retina.

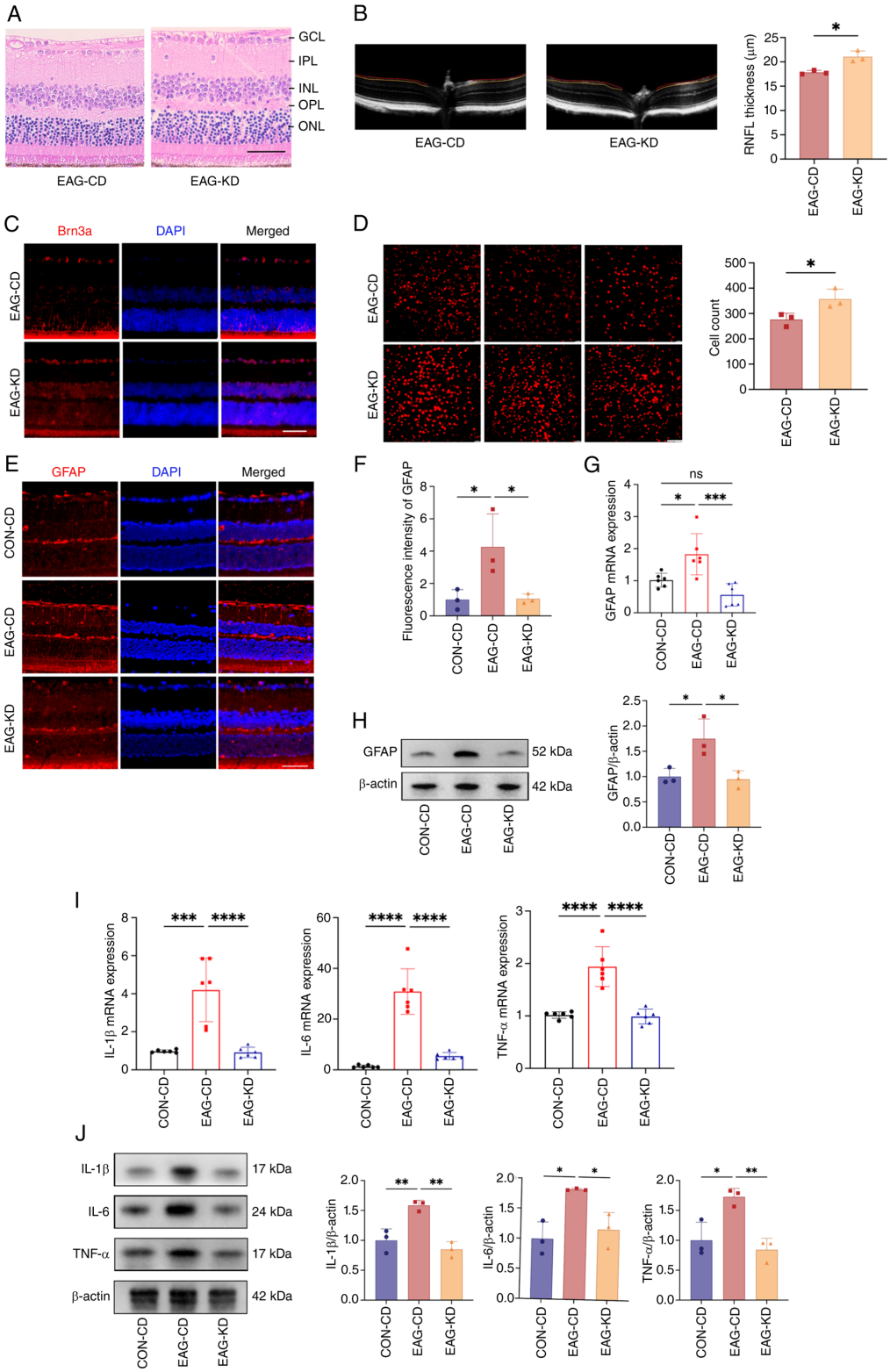

Figure 4. KD suppresses Müller cell activation and retinal inflammation in EAG mice. (A) H&E staining of retinal sections in EAG-CD and EAG-KD groups (n=3 mice for each group). (B) Optical coherence tomography analysis and quantification of RNFL thickness in EAG-CD and EAG-KD groups (n=3 mice for each group). (C) Immunofluorescent staining of Brn3a$^+$ cells in the retinal sections of EAG-CD and EAG-KD groups (n=3 mice for each group). (D) Immunofluorescent staining quantification data of Brn3a$^+$ cells in the retinal flat mounts of EAG-CD and EAG-KD groups (n=3 mice for each group). (E) Immunofluorescent staining and (F) quantification data of GFAP in the retinal sections of CON-CD, EAG-CD and EAG-KD groups (n=3 mice for each group). (G) Relative mRNA expression levels of GFAP in the retinas of CON-CD, EAG-CD and EAG-KD groups (n=6 mice for each group). (H) Western blotting analysis quantification of GFAP expression in the retinas of CON-CD, EAG-CD and EAG-KD groups (n=3 mice for each group). (I) Relative mRNA expression of IL-1β, IL-6 and TNF-α in the retinas of CON-CD, EAG-CD and EAG-KD groups (n=6 mice for each group). (J) Western blotting analysis quantification of IL-1β, IL-6 and TNF-α protein expressions in the retinas of CON-CD, EAG-CD and EAG-KD groups (n=3 mice for each group; scale bar, 50 μm). Data are presented as the mean ± SD. Unpaired t-tests were used for (B and D). One-way ANOVA was used for (F-J). *P<0.05, **P<0.01, ***P<0.001 and ****P<0.0001. ns, not significant; EAG, experimental autoimmune glaucoma; KD, ketogenic diet; CD, control diet; GFAP, glial fibrillary acidic protein; GCL, ganglion cell layer; IPL, inner plexiform layer; INL, inner nuclear layer; OPL, outer plexiform layer; ONL, outer nuclear layer; RNFL, retinal nerve fibre layer; Brn3a, brain-specific homeobox/POU domain protein 3A; EAG-KD, irradiated KD; EAG-CD, irradiated CD.

BHB suppresses Müller cell activation and inflammatory factors in vitro. To explore the role of BHB *in vitro*, primary Müller cells were isolated from neonatal mouse retinas and cultured. After 2-3 passages, the cells achieved high purity, as determined by their distinct morphology and positive immunofluorescence for GS (Fig. 5A; Fig. S2). Müller cell viability after 72 h of LPS stimulation was measured using a CCK-8 assay. Cell viability decreased significantly at all tested LPS concentrations >1 μg/ml (2, 5 and 10 μg/ml). Based on this, 1 μg/ml was chosen as the maximum concentration that did not compromise cell viability and was used for subsequent experiments (Fig. 5B). The effects of BHB on Müller cells were then evaluated with or without 1 μg/ml LPS. In the absence of LPS, BHB concentration up to be 20 mM did not significantly affect cell viability (Fig. 5C). Under LPS stimulation, no significant reduction in cell viability was observed at BHB concentrations up to 5 mM, whereas a significant decline occurred at 10 mM (Fig. 5D). Accordingly, 5 mM BHB was selected as the maximum non-toxic concentration for further experiments. After 72 h of LPS stimulation, MCT1 and OXCT1 expression was found to be significantly reduced in Müller cells compared with controls. In the LPS-stimulated cells treated with BHB, MCT1 and OXCT1 expression was significantly upregulated (Fig. 5E and F). Concurrently, LPS stimulation significantly increased GFAP expression in Müller cells and further significantly reduced it upon BHB treatment (Fig. 5G and H). Western blotting and RT-qPCR analyses showed that LPS-induced increases in IL-1β, IL-6 and TNF-α were significantly suppressed by BHB treatment (Fig. 5I and J). Collectively, these *in vitro* findings indicate that BHB is associated with reduced Müller cell activation and inflammatory factor secretion, consistent with the *in vivo* observations.

KD is associated with increased FOXO3A acetylation and MT2A expression in vivo and in vitro. KD exerts a similar inhibitory effect to a naturally occurring and specific inhibitor of class I histone deacetylases. Pan-acetylation was assessed by detecting overall acetylated lysine levels. KD feeding and BHB treatment restored the diminished global acetylation levels in the retinas of EAG mice and in LPS-stimulated Müller cells, respectively (Fig. 6A). Given the observed global increase in protein acetylation, 4D-DIA proteomic analysis was performed to pinpoint the specific proteins and pathways affected. Comparative analysis revealed distinct protein expression profiles among the control, LPS and LPS+BHB groups (Fig. 6B and C; Fig. S3A-D). A set of 76 proteins that were decreased in the LPS group relative to controls and increased in the LPS + BHB group was identified and visualized using a clustering heatmap (Fig. 6D; Table SV). Among these, proteins that met the criterion of fold change >1.2 and had a $P<0.05$ in paired comparisons were selected. FOXO3A and MT2A were found to be significantly upregulated and their expression differences are presented as a volcano plot and a box plot, respectively (Fig. 6E-G). GO and KEGG enrichment analyses revealed significant upregulation of the 'FoxO signalling pathway' following BHB treatment in LPS-stimulated cells. (Figs. 6H and S3E). Reactome analysis further supported the involvement of FOXO, with the most prominent enrichment observed in 'Regulation of FOXO transcriptional activity by acetylation' (Fig. 6I).

Western blotting analysis demonstrated that LPS significantly suppressed FOXO3A and MT2A expression, as well as FOXO3A acetylation at Lys271, in Müller cells and these effects were then significantly reversed by BHB treatment (Fig. 7A). Consistent with these *in vitro* findings, parallel results were observed in the retina of EAG mice following KD feeding (Fig. 7B). Acetylation at Lys290, another known acetylation site of FOXO3A, was also investigated. In retinal tissue, KD feeding significantly increased FOXO3A acetylation at Lys290, a change similar to the trend observed at Lys271. However, in cultured Müller cells, Lys290 acetylation was barely detectable and did not significantly change upon BHB treatment (Fig. S4). These results indicate that the protective effect of BHB on Müller cells was accompanied by increased FOXO3A acetylation at Lys271 and upregulation of MT2A.

Discussion

To the best of our knowledge, the present study was the first to show that serum ketone body levels were significantly lower in patients with POAG compared with healthy controls and patients with PACG. A similarly significant reduction was determined in the EAG model. The data further show that KD feeding elevates circulating BHB levels and increase the expression of ketone body transporters and metabolic enzymes, while suppressing Müller cell activation, attenuating neuroinflammation and preserving RGCs. These protective effects were accompanied by upregulation of the FOXO signalling pathway, suggesting FOXO3A acetylation is a potential mediator of the neuroprotective effects of KD in glaucoma (as summarised in Fig. 8).

Ketone bodies serve as a key alternative metabolic fuel across all domains of life. Accumulating evidence has emphasized their important roles in mammalian cell metabolism, homeostasis and signalling across diverse physiological and pathological contexts (14,34-36). The present findings demonstrated that, unlike in PACG, the specific decreases in BHB and AcAc levels in POAG suggest that its pathogenesis is modulated by ketone bodies through an IOP-independent mechanism. A previous gene set analysis indicated that mitochondrial ketone body synthesis and degradation were notably associated with POAG (37), but direct detection data to determine this association are lacking. The present study aimed to address this gap. Conversely, acute exposure to hypoxia may increase plasma ketone body metabolism (38). This difference may be attributable to the hypoxic metabolic disturbances in this acute-phase study (38) occurring during the acute phase of the disease, whereas the decreases in BHB and AcAc observed in the present study were associated with chronic pathological changes. Subsequently, an immune glaucoma model was established to investigate the role of ketone bodies *in vivo*. Given that oestrogen protects RGCs, male mice were used for the EAG model to eliminate this variable (39). EAG mice developed notable glaucomatous injury, as evidenced by RNFL thinning, RGC loss, glial activation and increased inflammatory cytokine release. Notably, decreased BHB and AcAc levels were observed, consistent with the trend observed in patients with POAG. Notably, decreased BHB and AcAc levels were also observed, consistent with the trend seen in patients with POAG. Thus, the EAG model is suitable for

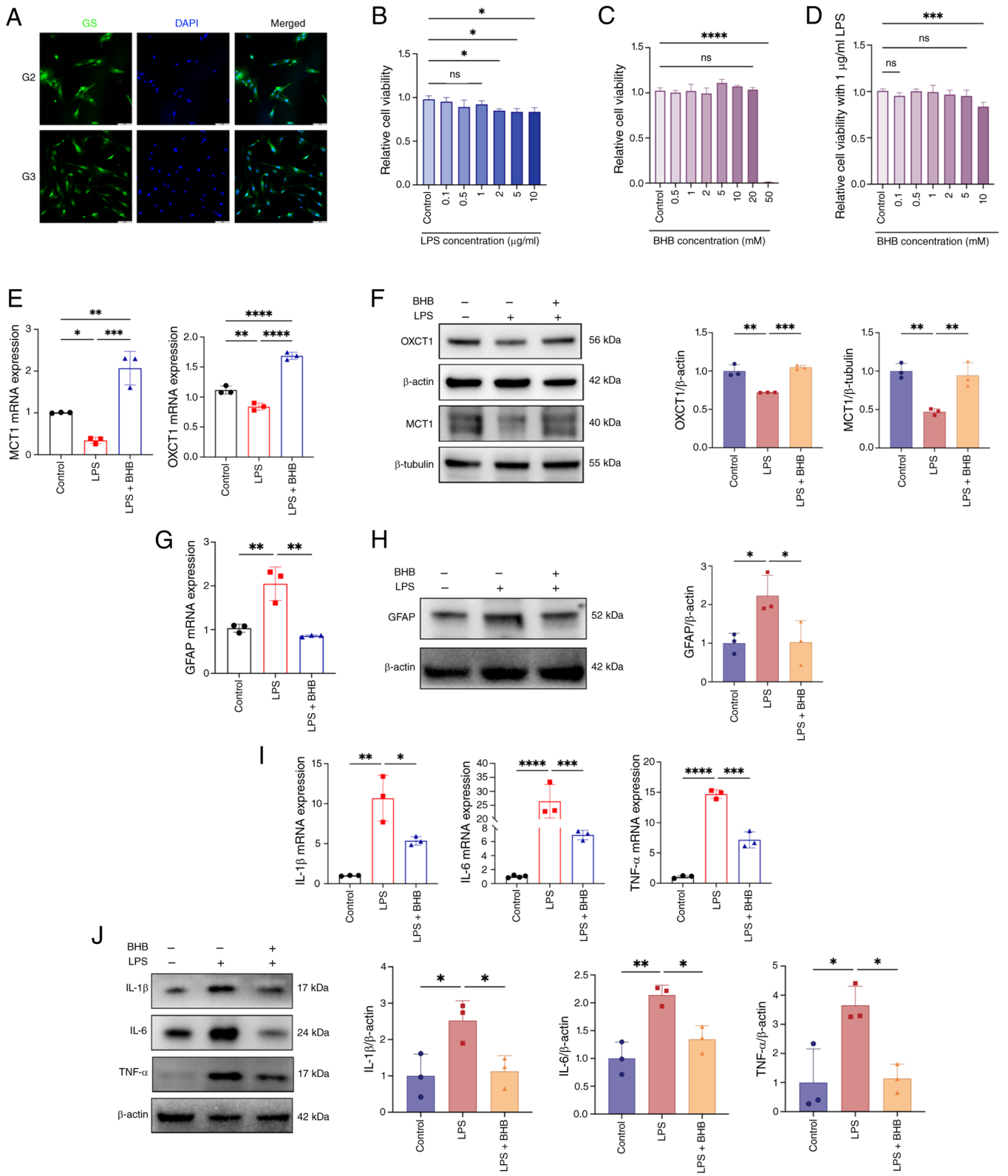

Figure 5. BHB enhances ketone body metabolism and suppresses expression of inflammatory factors in Müller cells. (A) Immunofluorescent staining of GS for identification in the primary Müller cells. (B) CCK-8 assay of cell viability in Müller cells treated with varying concentrations of LPS (n=3 cultures for each group). (C) CCK-8 assay of cell viability in Müller cells treated with varying concentrations of BHB alone (n=3 cultures for each group). (D) CCK-8 assay for cell viability in LPS-stimulated Müller cells treated with varying concentrations of BHB (n=3 cultures for each group). (E) Relative mRNA expression levels of MCT1 and OXCT1 in the control, LPS and LPS + BHB groups (n=3 cultures for each group). (F) Western blotting analysis and quantification of MCT1 and OXCT1 protein expressions in the control, LPS and LPS + BHB groups (n=3 cultures for each group). (G) Relative mRNA expression of GFAP in the control, LPS and LPS + BHB groups (n=3 cultures for each group). (H) Western blotting analysis and quantification of GFAP protein expression in the control, LPS and LPS + BHB groups (n=3 cultures for each group). (I) Relative mRNA expression of IL-1β, IL-6 and TNF-α in the control, LPS and LPS + BHB groups (n=3 cultures for each group). (J) Western blotting analysis and quantification of IL-1β, IL-6 and TNF-α protein expressions in the control, LPS and LPS + BHB groups (n=3 cultures for each group; scale bar, 50 μm). Data are presented as the mean ± SD. One-way ANOVA was used for all data analysis. *P<0.05, **P<0.01, ***P<0.001 and ****P<0.0001. ns, not significant; GS, glutamine synthetase; MCT, monocarboxylate transporter; OXCT1, 3-oxoacid CoA-transferase 1; CCK-8, Cell Counting Kit-8; GFAP, glial fibrillary acidic protein; BHB, β-hydroxybutyrate; LPS, lipopolysaccharide.

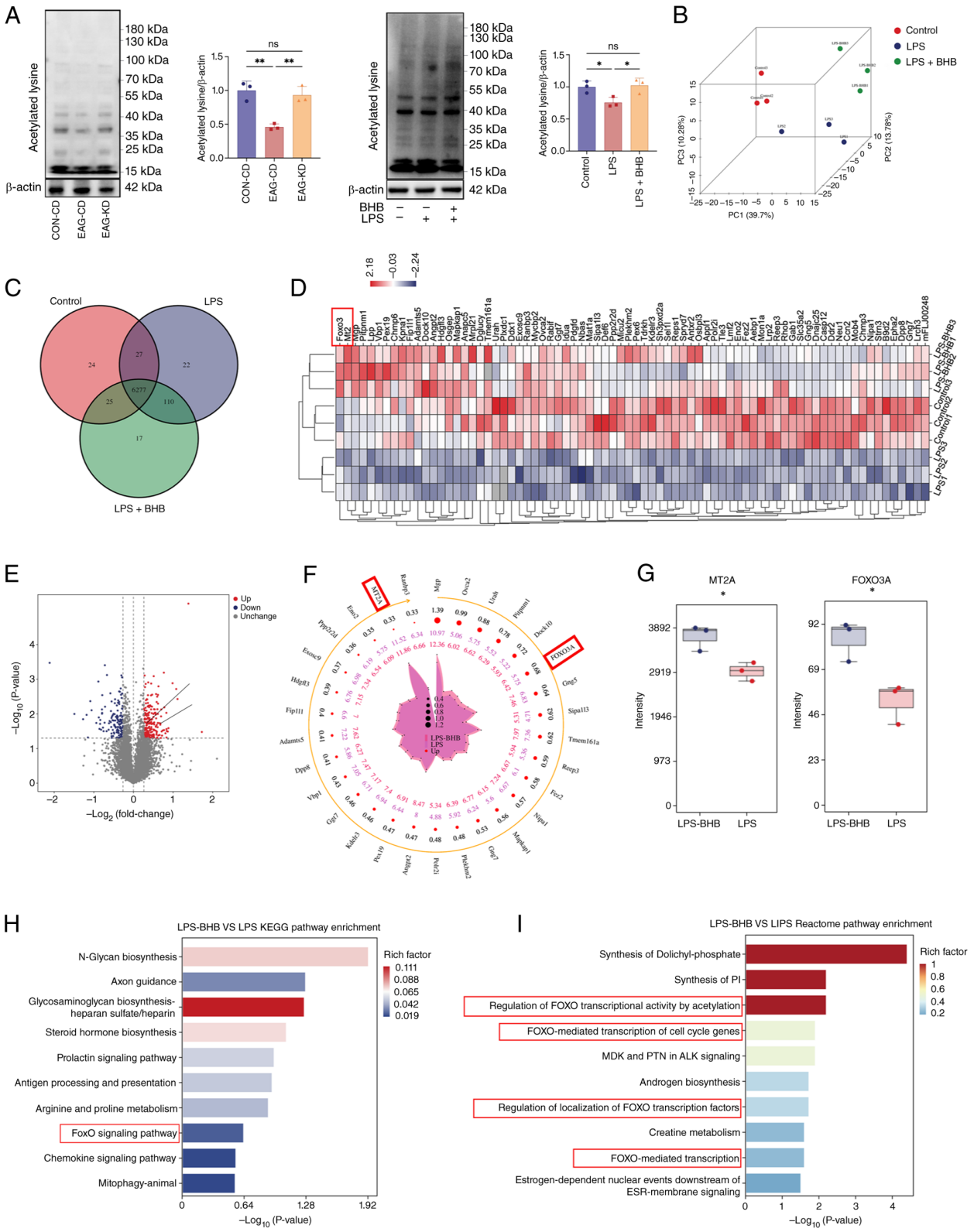

Figure 6. Proteomic analysis via 4D data-independent acquisition of Müller cells following BHB treatment under LPS stimulation. (A) Western blotting analysis and quantification of acetylation levels in the retinas of CON-CD, EAG-CD and EAG-KD groups of mice (n=3 mice for each group); and in the control, LPS and LPS + BHB groups of Müller cells (n=3 cultures for each group). (B) Plot indicating 3D principal component analysis of distribution of proteomic profiles among the control, LPS and LPS + BHB groups (n=3 cultures for each group). (C) Venn diagram showing the overlap of identified peaks among the three groups. (D) Clustering heatmap of the 76 proteins identified by a directional trend of decreased expression in the LPS group relative to control and increased expression in the LPS + BHB group relative to LPS (P<0.05). (E) Volcano plot and (F) radar plot displaying differentially expressed proteins, with FOXO3A and MT2A highlighted. Proteins shown met the criteria of fold change >1.2 and P<0.05 in pairwise comparisons. (G) Box plots showing the relative expression levels of FOXO3A and MT2A across the three groups (n=3 cultures for each group). (H) KEGG enrichment analysis of differential metabolic pathways between the LPS and LPS + BHB groups. (I) Reactome enrichment analysis of signal transduction mechanisms between the LPS and LPS + BHB groups. Data are presented as the mean ± SD. One-way ANOVA was used for (A and B). Unpaired t-tests were used for (G). *P<0.05 and **P<0.01. ns, not significant; KEGG, Kyoto Encyclopaedia of Genes and Genomes; BHB, β-hydroxybutyrate; LPS, lipopolysaccharide; CD, control diet; KD, ketogenic diet; MCT, monocarboxylate transporter; EAG-KD, irradiated KD; EAG-CD, irradiated CD; Up, upregulated; Down, downregulated.

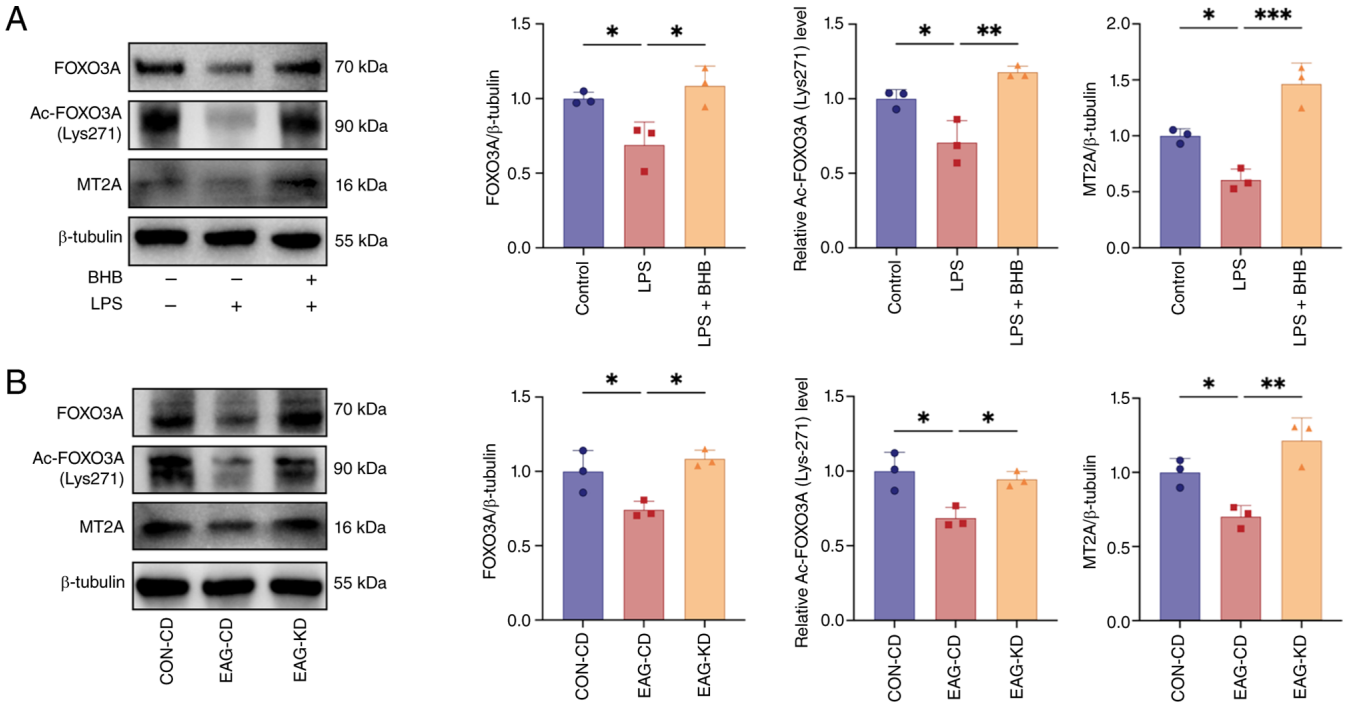

Figure 7. Expression of the FOXO3A, Ac-FOXO3A and MT2A proteins in EAG mice and primary Müller cells. (A) Western blotting analysis and quantification of FOXO3A, MT2A and FOXO3A acetylation at Lys271 in Müller cells from control, LPS and LPS + BHB groups (n=3 cultures for each group). (B) Western blotting analysis and quantification of FOXO3A, MT2A and Ac-FOXO3A at Lys271 in the retinas of CON-CD, EAG-CD and EAG-KD groups (n=3 mice for each group). Data are presented as the mean ± SD. One-way ANOVA was used for (A and B). *P<0.05, **P<0.01 and ***P<0.001. ns, not significant; Ac-, acetylation; MT2A, metallothionein 2A; CD, control diet; KD, ketogenic diet; EAG-KD, irradiated KD; EAG-CD, irradiated CD; BHB, β-hydroxybutyrate; LPS, lipopolysaccharide; EAG, experimental autoimmune glaucoma.

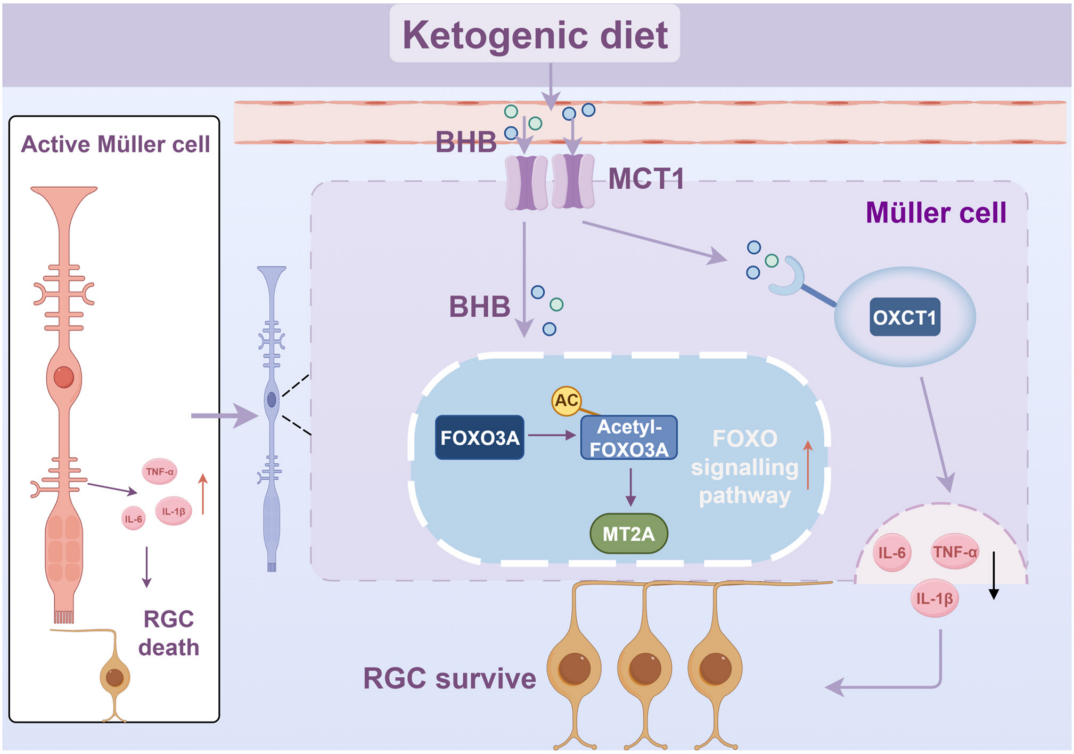

Figure 8. Illustration of the regulation of ketogenic diet and its underlying mechanism for reducing retinal immune-inflammation. Schematic created with Figdraw. RGC, retinal ganglion cell; BHB, β-hydroxybutyrate; MCT, monocarboxylate transporter; OXCT1, 3-oxoacid CoA-transferase 1; AC, acetyl group.

exploring the association between glaucomatous optic nerve injury and ketone bodies. These findings indicate that serum ketone body levels may serve as biomarkers for the diagnosis and assessment of glaucoma.

To investigate whether elevating ketone body levels could alleviate glaucomatous damage, a reliable and well-tolerated method of raising circulating ketone bodies is needed. KD drives sustained endogenous ketogenesis, producing a steady elevation of BHB along with AcAc and acetone, whereas exogenous BHB salts or esters tend to produce transient peaks and may cause gastrointestinal discomfort at higher doses (15,40). KD has also been used safely for decades in epilepsy and has been increasingly studied in other neurodegenerative conditions, including Alzheimer's disease, Parkinson's disease and multiple sclerosis (18), so its long-term feasibility is well established. Therefore, KD rather than direct BHB supplementation was chosen to raise circulating ketone body levels. A total of 4 weeks of KD feeding reliably raised serum ketone body levels in EAG mice, demonstrating that the dietary intervention was effective in the present study, with the most notable increase observed in BHB. In the present study, KD not only elevated serum ketone body levels but also enhanced ketone body transport, utilization, as well as overall ketone metabolism in the retina. Increased expression of MCT1 and OXCT1 was also detected, accompanied by minimal effects on MCT2 expression. The underlying reason for this difference may be that MCT1 exhibits a stronger affinity for ketone bodies than MCT2 (41). This observation aligns with a previous report that the hippocampus exhibited a robust response to nutritional ketosis in MCT1 and OXCT1 levels (42). Neuron-specific MCT1 upregulation alone can markedly promote axonal regeneration and improve recovery after spinal cord injury (43).

Previous studies have found that MCT1 is more abundantly expressed in the lactate shuttle between Müller cells and photoreceptors, whereas MCT2 is expressed in neuronal cells in the GCL and astrocytes (44,45). Müller cell activation, with the consequent release of inflammatory mediators, exacerbates RGC apoptosis in glaucoma (46). The present evidence suggested that KD inhibits GFAP and inflammatory mediator expression in the retinas of EAG mice, suggesting suppression of both Müller cell activation and retinal inflammation. Müller cells are key effector cells in retinal energy metabolism. MCT1 and OXCT1 were found to be localized predominantly in the retinal layers where Müller cells reside and their expression was regulated by KD, suggesting that Müller cells may serve a central role in ketone body transport and utilization within the retina. Based on the present results, it was hypothesized that the KD-induced increase in retinal ketone body metabolism is predominantly mediated by Müller cells. Thus, primary Müller cells were cultured and used for *in vitro* experiments, determining that BHB promotes ketone body metabolism while inhibiting Müller cell activation and release of inflammatory cytokines (IL-1β, IL-6 and TNF-α). These results support that the neuroprotection afforded by KD arises from the inhibition of Müller cell inflammation in the immune pathogenesis of glaucoma, consistent with previous findings (47,48).

Furthermore, previous studies have shown that KD increases histone acetylation and global protein acetylation levels (49,50). In addition, endogenous BHB, which increases after KD, has been reported to exert a similar inhibitory effect to hydroxycarboxylic acid 2 to suppress neuroinflammation and exerts neuroprotective effects (51). In the present study, broad elevation of protein acetylation was observed in the retina of EAG mice following KD feeding and in LPS-induced Müller cells treated with BHB. This shift in acetylation prompted investigation of specific downstream targets that might mediate the observed anti-inflammatory effects. Subsequently, 4D-DIA proteomic analysis identified significant enrichment of a number of FOXO-associated biological processes, including 'Regulation of FOXO transcriptional activity by acetylation', which aligned with the present focus on acetylation regulation. KEGG enrichment analysis further exhibited significant enrichment of the 'FOXO signalling pathway'. Within this pathway, FOXO3A and MT2A were among the proteins significantly upregulated by BHB treatment in Müller cells.

MT2A is a known downstream target gene of FOXO3A (52) and both molecules have established roles in anti-inflammatory responses and cytoprotection. MT2A contributes to these processes through multiple mechanisms, including inhibition of NF-κB activation (53), regulation of endothelial-overexpressed LPS-associated factor-1 (54), and suppression of pro-inflammatory cytokines such as IL-6, IL-12 and TNF-α (55). FOXO3A exerts anti-inflammatory effects by upregulating IκB expression and directly binding to NF-κB p65 to inhibit its transcriptional activity, thereby suppressing pro-inflammatory cytokines such as TNF-α, IL-1β and IL-6 (56). The FOXO family of transcription factors is predominantly regulated by acetylation or phosphorylation (57) and FOXO3A is known to be acetylated at numerous lysine residues, among which Lys271 and Lys290 have been the most extensively studied (58,59). In the present experiments, KD induced significant alterations in acetylated FOXO3A. Specifically, although changes were observed at both Lys271 and Lys290 in the retina, only the modification at Lys271 was detected in cultured Müller cells. The Lys290 signal was barely detectable above background levels, making reliable assessment difficult. This may imply that Lys290 acetylation is either less prominent in Müller cells or regulated independently of BHB and that Lys271 is the primary site through which BHB modulates FOXO3A activity in this cell type. This would be consistent with the concept that different FOXO acetylation sites can be differentially regulated depending on cell type and cellular context (60). The subsequent upregulation of MT2A, a known downstream target of FOXO3A, further supports the involvement of this pathway. Collectively, these findings suggest that KD elevates BHB levels and that the accompanying FOXO3A acetylation at Lys271 and MT2A upregulation are associated with activation of the FOXO signalling pathway. These changes may contribute to the attenuation of retinal neuroinflammation in glaucoma.

The present study exhibits a number of limitations that should be acknowledged. First, the present findings suggest that BHB could be a potential diagnostic biomarker for glaucoma. Despite this, methods for its quantification and detection in clinical diagnosis and therapy require further investigation. Second, direct *in vivo* administration of BHB was not performed in the present study. Therefore, whether BHB alone can fully recapitulate the neuroprotective effects of KD in the EAG model remains to be investigated. Third, mutating the acetylation sites of FOXO3A in Müller cells will help to clarify the functional contributions of each acetylation site. Therefore, future research should aim to focus on addressing these limitations and exploring other mechanisms of KD in the treatment of glaucoma, as well as promoting clinical applications and drug development.

In conclusion, the present study revealed an association between dysregulated ketone body metabolism and neuroinflammation in glaucoma. To the best of our knowledge, the present data provide the first evidence in EAG model that KD alleviates retinal neuroinflammation and attenuates Müller cell activation through acetylation-mediated FOXO signalling. These findings offer new insights into the role of metabolic regulation in neurodegenerative diseases, provide evidence for Müller cell phenotypic modulation and suggest potential avenues for metabolism-based neuroprotective strategies. KD and its key metabolite BHB warrant further investigation to explore their potential clinical applications in glaucoma treatment.

Acknowledgements

Not applicable.

Funding

The present study was supported by the Natural Science Foundation of Chongqing Municipality (grant no. CSTB2024NSCQ-KJZMSX0073), the National Natural Science Foundation of China (grant no. 82471064) and the Science and Technology Innovation Key R&D Program of Chongqing (grant no. CSTB2025TIAD-STX0008).

Availability of data and materials

The data generated in the present study may be found in the iProX database under accession number IPX0018867000 or at the following URL: https://www.iprox.cn/page/project.html?id=IPX0018867000.

Authors' contributions

SST and XCW contributed equally to the present study. SST and XCW conceptualized the present study and analyzed the data, performed the experiments, interpreted the results of the experiments and prepared the figures, wrote the original draft and reviewed and edited the manuscript. YFZ, ZNM, LHZ and JCY performed the experiments and analyzed the data. XCW, XF, MW, YJH and RTOY performed the investigation, visualization and conducted data validation. YYP, JQL, XG, DDW and YP recruited the samples. HL conceptualized the present study, handled supervision and acquired the funding. SST, XCW and HL confirm the authenticity of all the raw data. All authors read and approved the final version of the manuscript and are accountable for all aspects of the work.

Ethics approval and consent to participate

The guiding principles of the Declaration of Helsinki were strictly followed in all procedures. The clinical research process was approved by the Ethical Committee of the First Affiliated Hospital at Chongqing Medical University (Chongqing, China; approval no. 2024-087-01). Written informed consent was obtained from all participants involved in the research. All animal research was supported by the Institutional Animal Care and Use of Chongqing Medical University (Chongqing, China; approval no. IACUC-CQMU-2025-0349) and in compliance with Association for Research in Vision and Ophthalmology guidelines.

Patient consent for publication

Not applicable.

Competing interests

The authors declare that they have no competing interests.

References

1. Cao Y, Yin X, Wu L, Huang D, Wang Z, Wu F, Jiang J, Chen G and Wang Q: High-efficiency ocular delivery of brain-derived neurotrophic factor and oligomycin for neuroprotection in glaucoma. Adv Mater 37: e2500623, 2025.
2. Tham YC, Li X, Wong TY, Quigley HA, Aung T and Cheng CY: Global prevalence of glaucoma and projections of glaucoma burden through 2040: A systematic review and meta-analysis. Ophthalmology 121: 2081-2090, 2014.
3. Chang YF, Cheng YH, Ko YC, Chiou SH and Liu CJ: Anti-apoptotic and autophagic effect: Using conditioned medium from human bone marrow mesenchymal stem cells to treat human trabecular meshwork cells. Regen Ther 22: 50-58, 2022.
4. Bartollino S, Chiosi F, di Staso S, Uva M, Pascotto A, Rinaldi M, Hesselink JMK and Costagliola C: The retinoprotective role of phenytoin. Drug Des Devel Ther 12: 3485-3489, 2018.
5. Baudouin C, Kolko M, Melik-Parsadaniantz S and Messmer EM: Inflammation in glaucoma: From the back to the front of the eye, and beyond. Prog Retin Eye Res 83: 100916, 2021.
6. Tian H, Chen Y, Zhao T, Ye L, Li H, Li Z, Qiu W, Wang W, Li R, Liu F, *et al*: Single-cell RNA-seq reveals cell type-specific molecular and genetic associations with primary open-angle glaucoma. Signal Transduct Target Ther 10: 338, 2025.
7. Geyer O and Levo Y: Glaucoma is an autoimmune disease. Autoimmun Rev 19: 102535, 2020.
8. Vecino E, Rodriguez FD, Ruzafa N, Pereiro X and Sharma SC: Glia-neuron interactions in the mammalian retina. Prog Retin Eye Res 51: 1-40, 2016.
9. Reichenbach A and Bringmann A: New functions of Müller cells. Glia 61: 651-678, 2013.
10. Xue LP, Lu J, Cao Q, Hu S, Ding P and Ling EA: Müller glial cells express nestin coupled with glial fibrillary acidic protein in experimentally induced glaucoma in the rat retina. Neuroscience 139: 723-732, 2006.
11. Goldman D: Müller glial cell reprogramming and retina regeneration. Nat Rev Neurosci 15: 431-442, 2014.
12. Penn JS, Madan A, Caldwell RB, Bartoli M, Caldwell RW and Hartnett ME: Vascular endothelial growth factor in eye disease. Prog Retin Eye Res 27: 331-371, 2008.
13. Miao Y, Zhao GL, Cheng S, Wang Z and Yang XL: Activation of retinal glial cells contributes to the degeneration of ganglion cells in experimental glaucoma. Prog Retin Eye Res 93: 101169, 2023.
14. Williams MS and Turos E: The chemistry of the ketogenic diet: Updates and opportunities in organic synthesis. Int J Mol Sci 22: 5230, 2021.
15. Newman JC and Verdin E: β-Hydroxybutyrate: A signaling metabolite. Annu Rev Nutr 37: 51-76, 2017.
16. Lopa C, Pietrangelo D, Santulli G, Gambardella J, Rubattu S, Stefan-Lifshitz M, Garcia CN, Jankauskas SS and Lombardi A: Pancreas meets brain: β-hydroxybutyrate as a novel 'β-cellular' metabolism therapy. Metabolism 174: 156419, 2025.
17. McNally MA and Hartman AL: Ketone bodies in epilepsy. J Neurochem 121: 28-35, 2012.
18. Dynka D, Kowalcze K and Paziewska A: The role of ketogenic diet in the treatment of neurological diseases. Nutrients 14: 5003, 2022.
19. Tsusaka T, Najar MA, Schwarz B, Bohrnsen E, Oses-Prieto JA, Neudorf H, Lee C, Little JP, Burlingame AL, Bosio CM, *et al*: Reversible histone deacetylase activity catalyzes lysine acylation. Nat Chem Biol 21: 1387-1396, 2025.
20. Offermanns S: Hydroxy-carboxylic acid receptor actions in metabolism. Trends Endocrinol Metab 28: 227-236, 2017.

21. Shippy DC, Wilhelm C, Viharkumar PA, Raife TJ and Ulland TK: β-Hydroxybutyrate inhibits inflammasome activation to attenuate Alzheimer's disease pathology. J Neuroinflammation 17: 280, 2020.
22. Sun W, Wen M, Liu M, Wang Q, Liu Q, Li L, Siebert HC, Loers G, Zhang R and Zhang N: Effect of β-hydroxybutyrate on behavioral alterations, molecular and morphological changes in CNS of multiple sclerosis mouse model. Front Aging Neurosci 14: 1075161, 2022.
23. Deng M, Fang Y, Chu Y, Ding R, Fan X, Wei H, Song H, Jiang G, Zhang H, Han C and Yuan H: SIRT3 is required for the protective function of ketogenic diet on neural inflammation and neuropathic pain. Int J Biol Sci 21: 3011-3029, 2025.
24. Stein JD, Khawaja AP and Weizer JS: Glaucoma in adults-screening, diagnosis, and management: A review. JAMA 325: 164-174, 2021.
25. Wang M, Shen LQ, Pasquale LR, Petrakos P, Formica S, Boland MV, Wellik SR, De Moraes CG, Myers JS, Saeedi O, *et al*: An artificial intelligence approach to detect visual field progression in glaucoma based on spatial pattern analysis. Invest Ophthalmol Vis Sci 60: 365-375, 2019.
26. Association for Research in Vision and Ophthalmology (ARVO): ARVO statement for the use of animals in ophthalmic and vision research. ARVO, Rockville, MD, 2024.
27. Wiemann S, Reinhard J, Reinehr S, Cibir Z, Joachim SC and Faissner A: Loss of the extracellular matrix molecule tenascin-C leads to absence of reactive gliosis and promotes anti-inflammatory cytokine expression in an autoimmune glaucoma mouse model. Front Immunol 11: 566279, 2020.
28. Laspas P, Gramlich OW, Müller HD, Cuny CS, Gottschling PF, Pfeiffer N, Dick HB, Joachim SC and Grus FH: Autoreactive antibodies and loss of retinal ganglion cells in rats induced by immunization with ocular antigens. Invest Ophthalmol Vis Sci 52: 8835-8848, 2011.
29. Liu X, Tang L and Liu Y: Mouse Müller cell isolation and culture. Bio Protoc 7: e2429, 2017.
30. Zheng Y, Mou Z, Tan S, Wang X, Yuan J and Li H: IL-17A enhances the inflammatory response of glaucoma through Act1/TRAF6/NF-κB pathway. Neurochem Int 178: 105787, 2024.
31. Wiśniewski JR, Zougman A, Nagaraj N and Mann M: Universal sample preparation method for proteome analysis. Nat Methods 6: 359-362, 2009.
32. Yang L, Xu Z, Wang Z, Ding F, Wu Z, Shi X, Wang J, Ma Y and Jin J: Increased pro-SFTPB in HDL promotes the pro-inflammatory transition of HDL and represents a sign of poor prognosis in ARDS patients. J Transl Med 23: 75, 2025.
33. Livak KJ and Schmittgen TD: Analysis of relative gene expression data using real-time quantitative PCR and the 2(-Delta Delta C(T)) method. Methods 25: 402-408, 2001.
34. Tsuruta H, Yamahara K, Yasuda-Yamahara M and Kume S: Emerging pathophysiological roles of ketone bodies. Physiology (Bethesda) 39: 0, 2024.
35. Yurista SR, Nguyen CT, Rosenzweig A, de Boer RA and Westenbrink BD: Ketone bodies for the failing heart: Fuels that can fix the engine? Trends Endocrinol Metab 32: 814-826, 2021.
36. Cai W, Chong K, Huang Y, Huang C and Yin L: Empagliflozin improves mitochondrial dysfunction in diabetic cardiomyopathy by modulating ketone body metabolism and oxidative stress. Redox Biol 69: 103010, 2024.
37. Khawaja AP, Cooke Bailey JN, Kang JH, Allingham RR, Hauser MA, Brilliant M, Budenz DL, Christen WG, Fingert J, Gaasterland D, *et al*: Assessing the association of mitochondrial genetic variation with primary open-angle glaucoma using gene-set analyses. Invest Ophthalmol Vis Sci 57: 5046-5052, 2016.
38. Langbøl M, Rovelt J, Saruhanian A, Saruhanian S, Tiedemann D, Baskaran T, Bocca C, Vohra R, Cvenkel B, Lenaers G and Kolko M: Distinct metabolic profiles of ocular hypertensives in response to hypoxia. Int J Mol Sci 25: 195, 2023.
39. Reichstein D, Ren L, Filippopoulos T, Mittag T and Danias J: Apoptotic retinal ganglion cell death in the DBA/2 mouse model of glaucoma. Exp Eye Res 84: 13-21, 2007.
40. Stubbs BJ, Cox PJ, Evans RD, Santer P, Miller JJ, Faull OK, Magor-Elliott S, Hiyama S, Stirling M and Clarke K: On the metabolism of exogenous ketones in humans. Front Physiol 8: 848, 2017.
41. Begley DJ: 9-Efflux mechanisms in the central nervous system: A powerful influence on drug distribution within the brain. In: Sharma HS and Westman J (eds). Blood-Spinal Cord and Brain Barriers in Health and Disease. Academic Press: San Diego, CA, USA, pp83-97, 2004.
42. Liśkiewicz D, Liśkiewicz A, Nowacka-Chmielewska MM, Grabowski M, Pondel N, Grabowska K, Student S, Barski JJ and Małecki A: Differential response of hippocampal and cerebrocortical autophagy and ketone body metabolism to the ketogenic diet. Front Cell Neurosci 15: 733607, 2021.
43. Shi C, Xu J, Ding Y, Chen X, Yuan F, Zhu F, Duan C, Hu J, Lu H, Wu T and Jiang L: MCT1-mediated endothelial cell lactate shuttle as a target for promoting axon regeneration after spinal cord injury. Theranostics 14: 5662-5681, 2024.
44. Bergersen L, Jóhannsson E, Veruki ML, Nagelhus EA, Halestrap A, Sejersted OM and Ottersen OP: Cellular and subcellular expression of monocarboxylate transporters in the pigment epithelium and retina of the rat. Neuroscience 90: 319-331, 1999.
45. Yamagishi H, Kirai N, Morita A, Kashihara T and Nakahara T: Role of monocarboxylate transporters in AMPK-mediated protection against excitotoxic injury in the rat retina. Eur J Pharmacol 970: 176510, 2024.
46. Li Q, Cheng Y, Zhang S, Sun X and Wu J: TRPV4-induced Müller cell gliosis and TNF-α elevation-mediated retinal ganglion cell apoptosis in glaucomatous rats via JAK2/STAT3/NF-κB pathway. J Neuroinflammation 18: 271, 2021.
47. Gough SM, Casella A, Ortega KJ and Hackam AS: Neuroprotection by the ketogenic diet: Evidence and controversies. Front Nutr 8: 782657, 2021.
48. Yang H, Shan W, Zhu F, Wu J and Wang Q: Ketone bodies in neurological diseases: Focus on neuroprotection and underlying mechanisms. Front Neurol 10: 585, 2019.
49. Whatley EG, Harvey AJ and Gardner DK: A maternal ketogenic diet alters oviduct fluid nutrients and embryo histone acetylation in mice. Reproduction 167: e240026, 2024.
50. Roberts MN, Wallace MA, Tomilov AA, Zhou Z, Marcotte GR, Tran D, Perez G, Gutierrez-Casado E, Koike S, Knotts TA, *et al*: A ketogenic diet extends longevity and healthspan in adult mice. Cell Metab 27: 1156, 2018.
51. Rahman M, Muhammad S, Khan MA, Chen H, Ridder DA, Müller-Fielitz H, Pokorná B, Vollbrandt T, Stölting I, Nadrowitz R, *et al*: The β-hydroxybutyrate receptor HCA2 activates a neuroprotective subset of macrophages. Nat Commun 5: 3944, 2014.
52. Kops GJPL, Dansen TB, Polderman PE, Saarloos I, Wirtz KWA, Coffer PJ, Huang TT, Bos JL, Medema RH and Burgering BM: Forkhead transcription factor FOXO3a protects quiescent cells from oxidative stress. Nature 419: 316-321, 2002.
53. Takano H, Inoue K, Yanagisawa R, Sato M, Shimada A, Morita T, Sawada M, Nakamura K, Sanbongi C and Yoshikawa T: Protective role of metallothionein in acute lung injury induced by bacterial endotoxin. Thorax 59: 1057-1062, 2004.
54. Leng W, Lei X, Meng H, Ouyang X and Liang Z: EOLA1 inhibits lipopolysaccharide-induced vascular cell adhesion molecule-1 expression by association with MT2A in ECV304 cells. Int J Inflamm 2015: 301562, 2015.
55. Kim B, Kim HY, Yoon BR, Yeo J, In Jung J, Yu KS, Kim HC, Yoo SJ, Park JK, Kang SW and Lee WW: Cytoplasmic zinc promotes IL-1β production by monocytes and macrophages through mTORC1-induced glycolysis in rheumatoid arthritis. Sci Signal 15: eabi7400, 2022.
56. Cao G, Lin M, Gu W, Su Z, Duan Y, Song W, Liu H and Zhang F: The rules and regulatory mechanisms of FOXO3 on inflammation, metabolism, cell death and aging in hosts. Life Sci 328: 121877, 2023.
57. Liu W, Meng P, Li Z, Shen Y, Meng X, Jin S and Hu M: The multifaceted impact of physical exercise on FoxO signaling pathways. Front Cell Dev Biol 13: 1614732, 2025.
58. Leem YH, Park JS, Park JE, Kim DY and Kim HS: Creatine supplementation with exercise reduces α-synuclein oligomerization and necroptosis in Parkinson's disease mouse model. J Nutr Biochem 126: 109586, 2024.
59. Lu W, Deng Y, Liu M, Hu Y, Yang K, Wang B, Li Y, Wang G, Ma L, Liu J, *et al*: Regulation of apoptosis, ferroptosis, and pyroptosis mediated by acetylation. Cell Death Discov 12: 15, 2026.
60. Calnan DR and Brunet A: The FoxO code. Oncogene 27: 2276-2288, 2008.